Supplement of Atmos. Chem. Phys., 26, 8839–8854, 2026
https://doi.org/10.5194/acp-26-8839-2026-supplement

Atmospheric Chemistry and Physics
Open Access
EGU

Supplement of

Observations of nanoparticle shrinkage phenomena

Vijay P. Kanawade et al.

Correspondence to: Vijay P. Kanawade (v.kanawade@cyi.ac.cy) and Tuija Jokinen (t.jokinen@cyi.ac.cy)

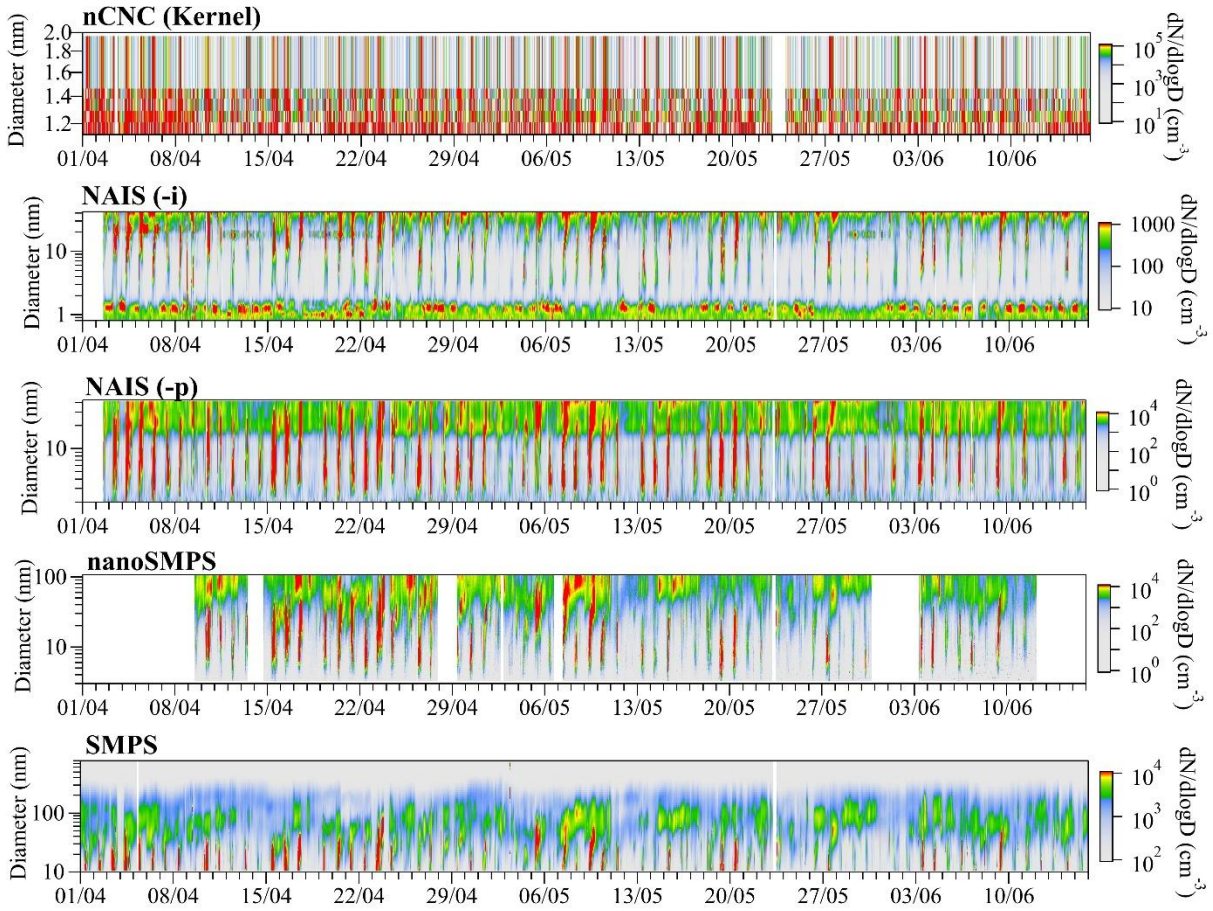

Figure S1. Time evolution of 10-minute median particle size distributions during the SPICY campaign, 1 April – 15 June 2024, based on nCNC, NAIS (negative polarity ions and particles), nano-DMA SMPS, and SMPS measurements.

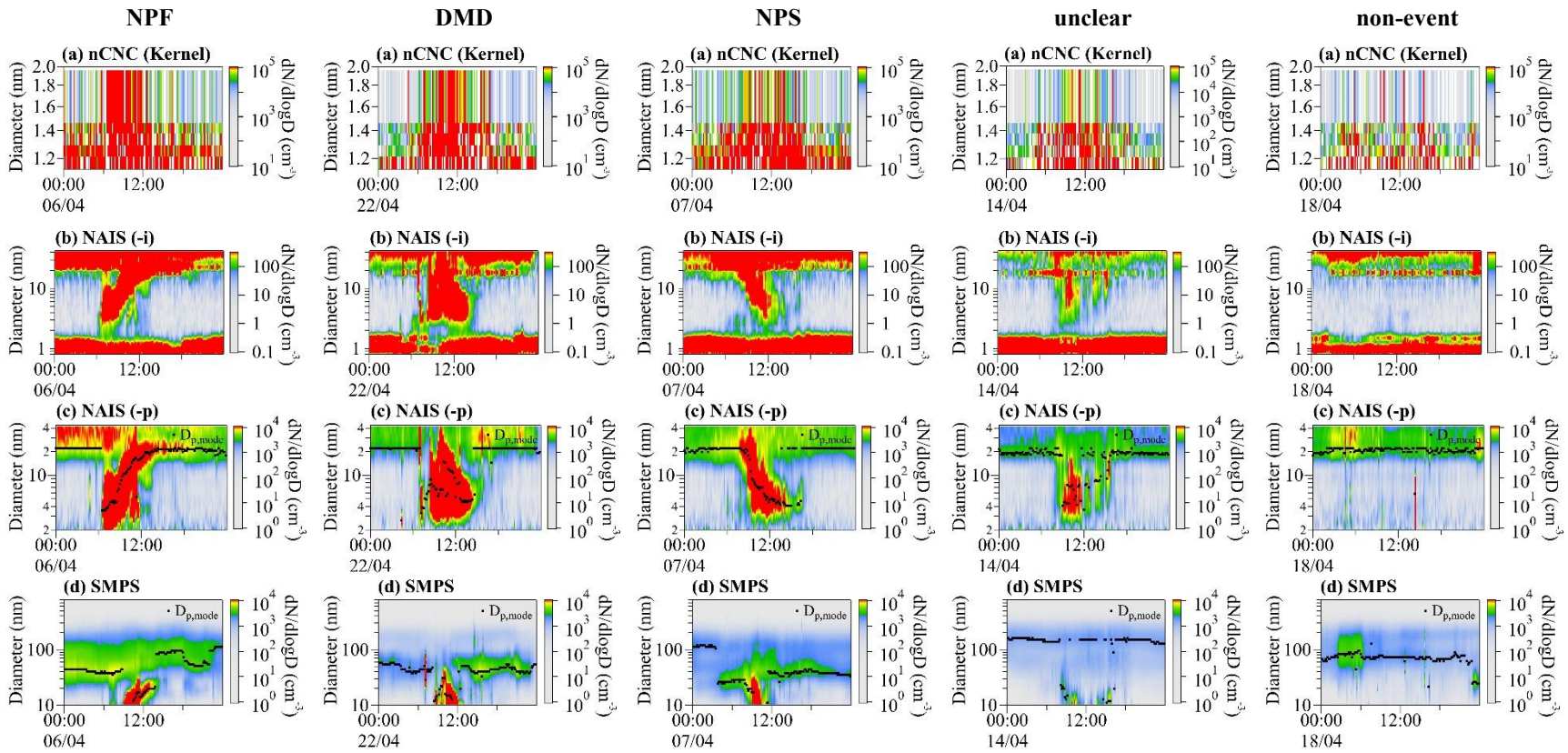

Figure S2. Median diurnal variation of particle size distributions measured by (a) nCNC, NAIS negative polarity (b) ions and (c) particles, and (d) SMPS for observed typical NPF, DMD, NPS, unclear and non-event days. Black dots indicate the particle mode diameter.

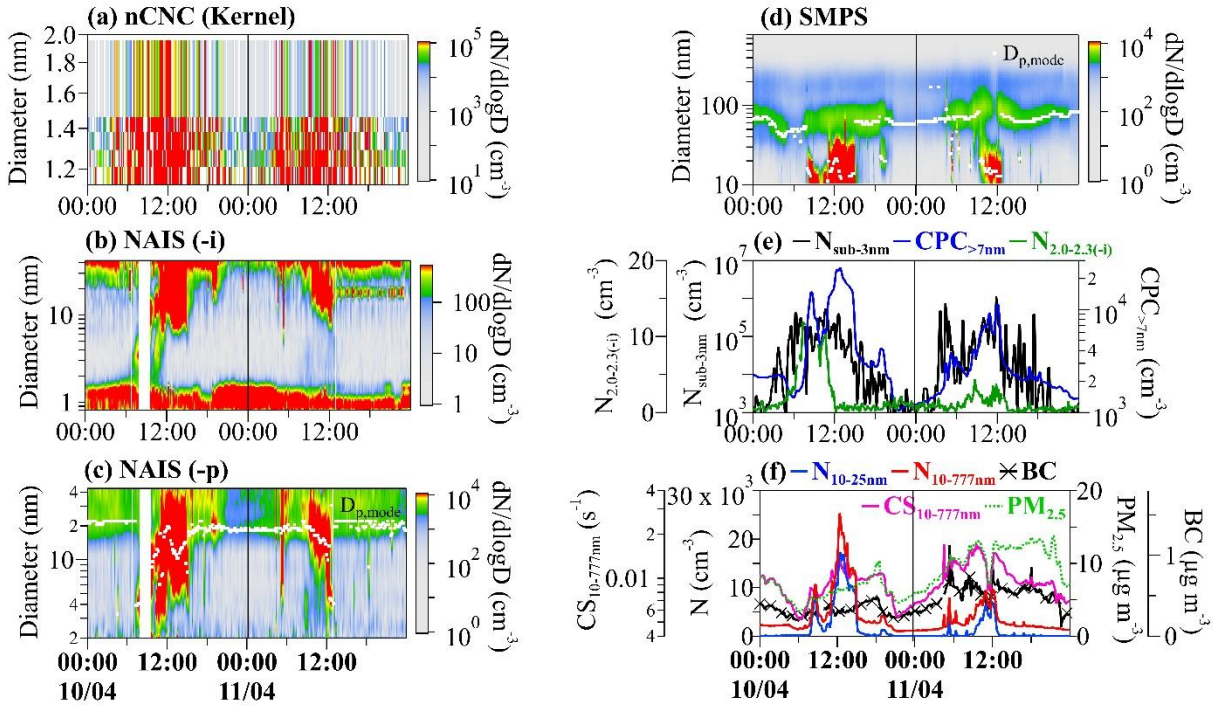

Figure S3. Median diurnal variation of aerosol properties during the consecutive NPF-NPS events observed during 10-11 April. Particle size distributions measured by (a) nCNC, (b-c) NAIS negative polarity ions and particles, and (d) SMPS. Panel (e) shows concentrations of negative polarity ions in the 2.0-2.3 nm size range measured by NAIS ($N_{2\text{-}2.3(\text{-}i)}$), sub-3nm particles measured by nCNC ($N_{sub\text{-}3nm}$), and >7nm particles measured by CPC ($N_{>7nm}$). Panel (f) shows nucleation mode ($N_{10\text{-}25nm}$) and total particle ($N_{10\text{-}777nm}$) number concentrations from SMPS, total condensation sink ($CS_{10\text{-}777nm}$), and particulate matter of aerodynamic diameter less than 2.5 μm ($PM_{2.5}$) and black carbon (BC) mass concentrations.

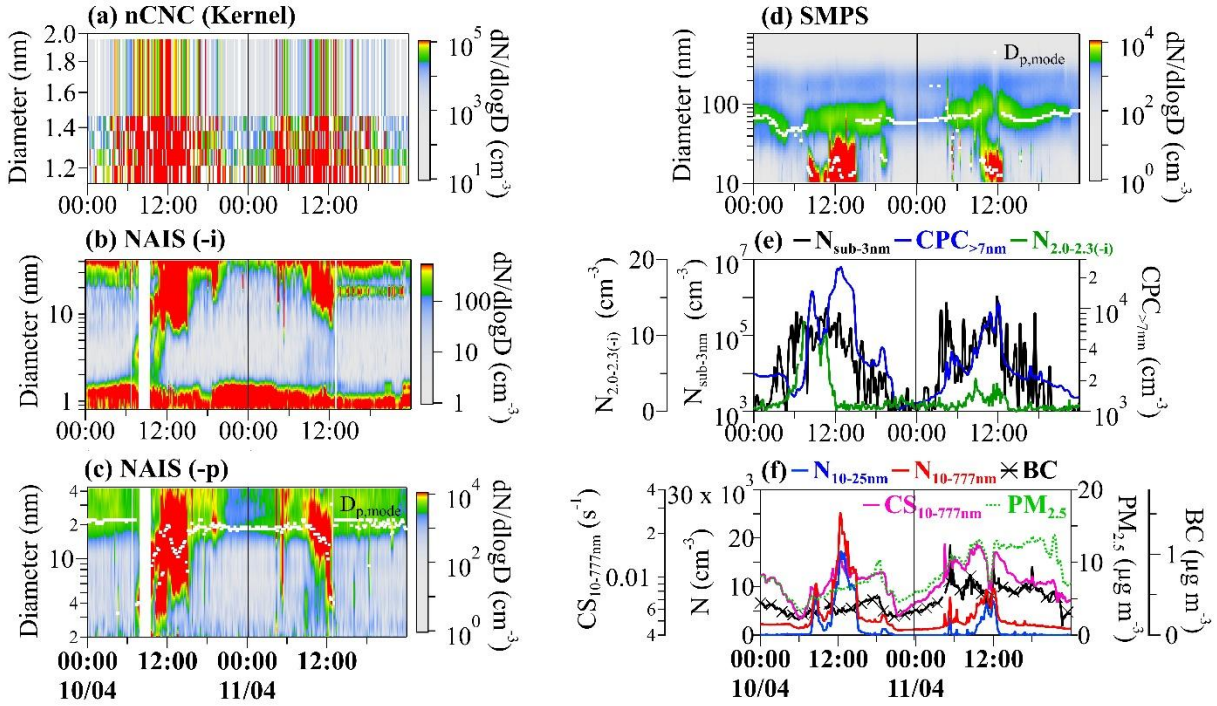

Figure S4. Same as Fig. S3, but for the consecutive NPF-NPS events observed during 20-21 April.

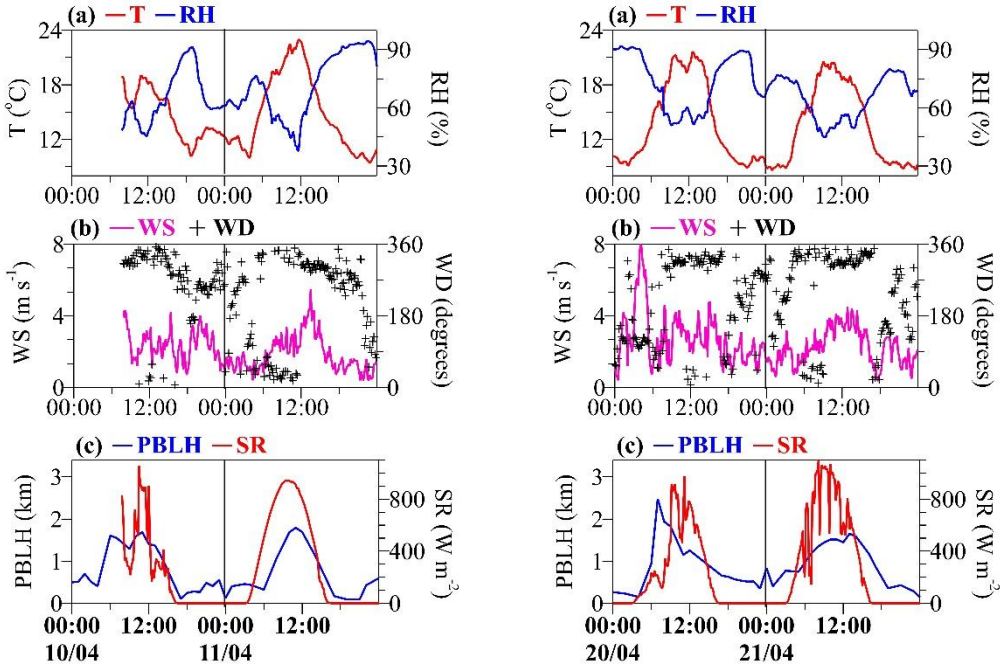

Figure S5. Median diurnal variation of meteorological parameters during the consecutive NPF-NPS events, shown for the 10-11 April case (left panel) and the 20-21 April case (right panel). (a) air temperature and relative humidity, (b) wind speed and wind direction, and (c) planetary boundary layer height and solar radiation.

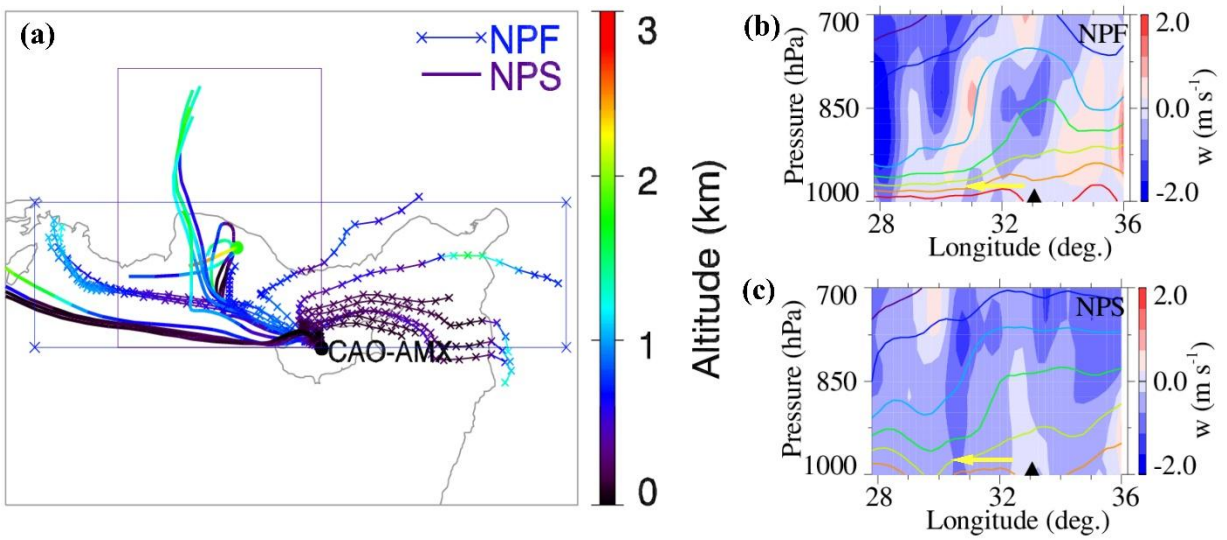

Figure S6. 48-hour air-mass backward trajectories (0-12 UTC) as a function of altitude, initialized at 500 meters above ground level at the AMX site during the NPF event (10 April, line connected by cross symbol) and the NPS event (11 April, solid lines. The region shown by the rectangular box is used to create longitude (latitude)-altitude cross-sections of averaged (b-c) vertical velocity (w, filled contours) along air-mass trajectories over 0-9 UTC for NPF and NPS event days observed on 10 April and 11 April, respectively. Contour lines represent specific humidity of 2, 3, 4, 5, 6, 7, 8, and 10 g kg^{-1}, shown in black, violet, blue, cyan, green, yellow, orange, and red, respectively. The negative value of w indicates subsidence, while the positive values indicate the updraft. The yellow-colored arrows indicate the upwind region of the measurement site.

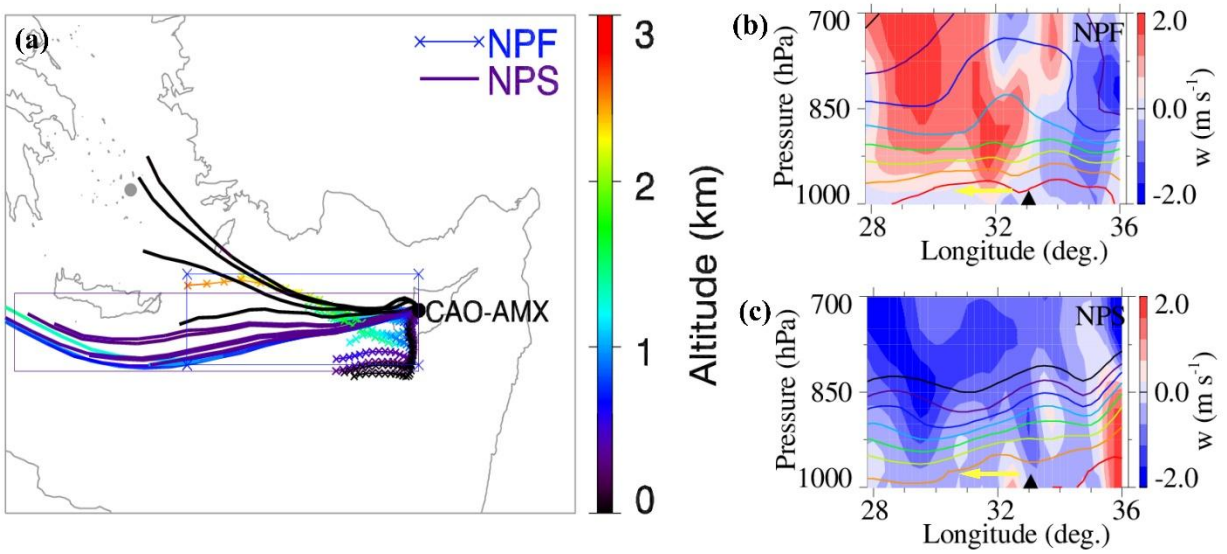

Figure S7. Same as Fig. S6, but for the consecutive NPF-NPS events observed during 20-21 April.

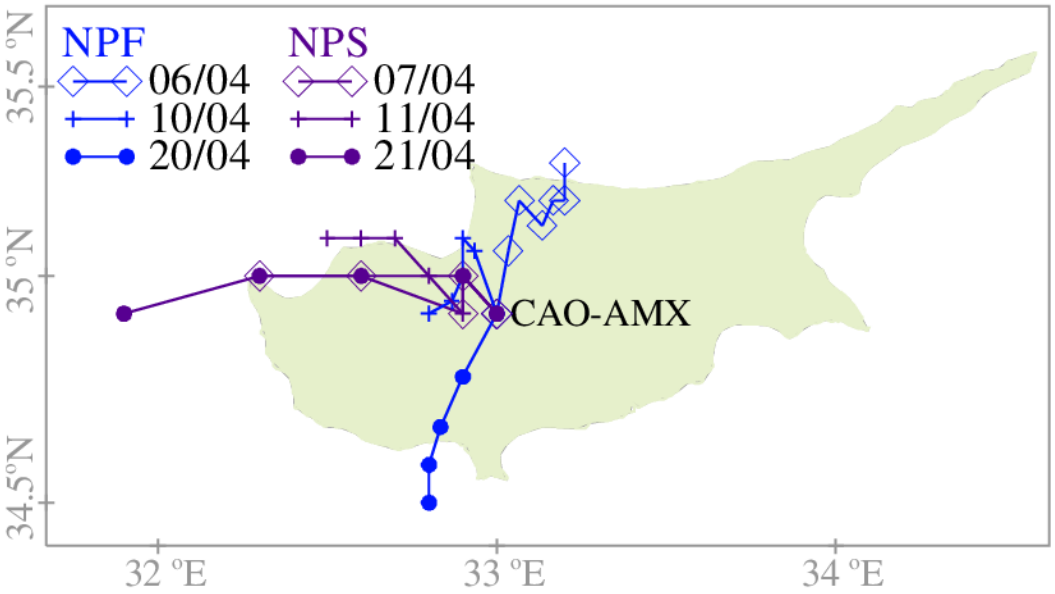

Figure S8. Spatial extent of the observed NPF (blue lines) and NPS (purple lines) events. The spatial coverage of each event was estimated using hourly air-mass backward trajectories following the methodology described by Hussein et al. (2009). For each event, the starting time was defined as 06:00 UTC and the ending time as 12:00 UTC, based on the visualisation of contour plots of particle size distribution from the NAIS (Fig. 3b). Hourly backward air-mass trajectories were traced in the upwind direction between 6:00 and 12:00 UTC, representing the possible regions where the event may have been triggered. Each trajectory represents the approximate geographical coverage of an event.

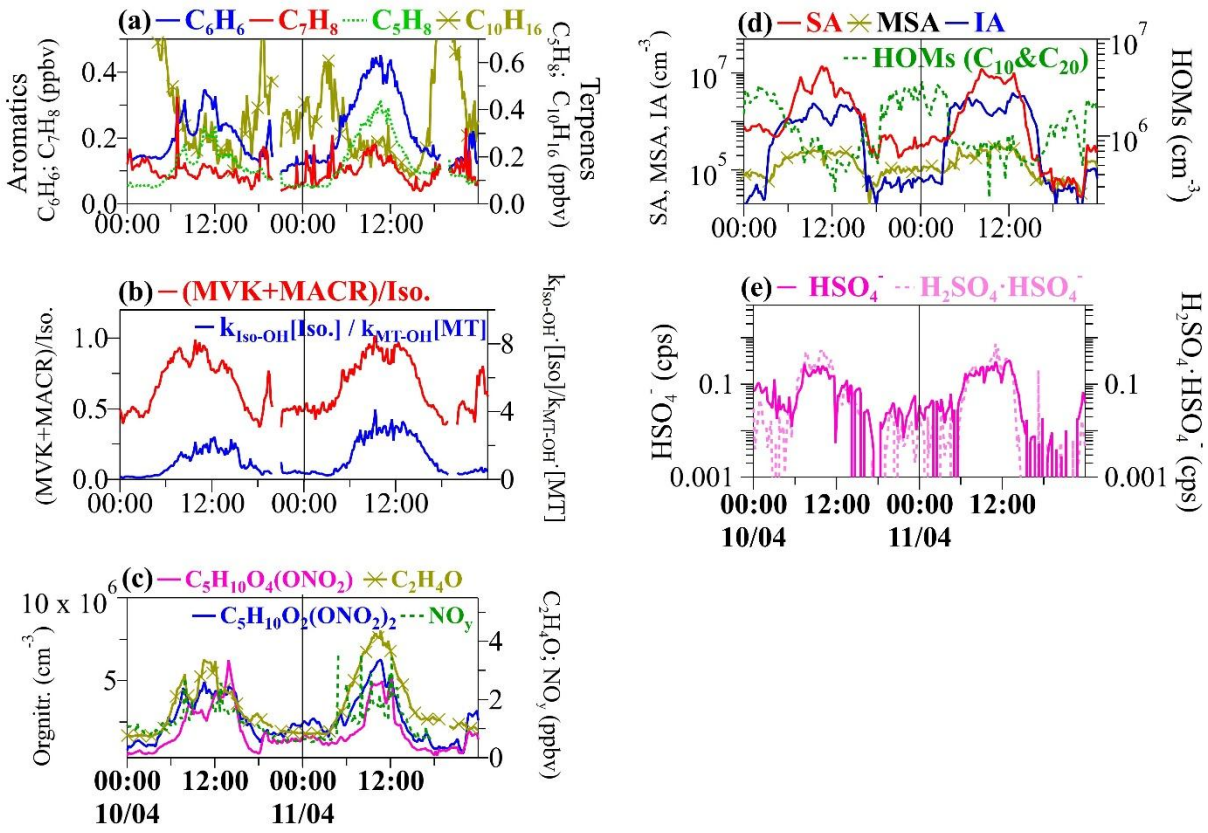

Figure S9. Median diurnal variation of aerosol precursors and condensing vapours during the consecutive NPF-NPS events observed during 10-11 April. (a) mixing ratios of benzene (C_6H_6), toluene (C_7H_8), isoprene (C_5H_8), and monoterpenes ($C_{10}H_{16}$); (b) the ratio of sum of methyl vinyl ketone (MVK) and maethacrolein (MACR) to the isoprene [(MVK+MACR)/Iso.] and the relative OH reaction rates of isoprene and MTs ($k_{Iso\text{-}OH}\cdot[Iso]/k_{MT\text{-}OH}\cdot[MT]$); (c) organonitrates ($C_5H_{10}O_4(ONO_2)$ and $C_5H_{10}O_2(ONO_2)_2$), acetaldehyde (C_2H_4O) and reaction nitrogen compounds (NO_y); (d) concentrations of sulfuric acid (SA), methyl sulfonic acid (MSA), iodic acid (IA), and highly oxygenated organic molecules (HOMs, C_{10} & C_{20}); (e) ambient ion mode signals of bisulfate monomer (HSO_4^-)and dimer ($H_2SO_4 \cdot HSO_4^-$) in counts per second (cps); (f) the percentage difference in organic vapour concentrations (molecules cm^{-3}) between the NPF and NPS events as a function of volatility bin, expressed as $\log_{10}$ of the effective saturation concentration, $\log_{10}(C^*)$. Negative percentage differences indicate higher organic vapour concentrations during the NPS event. ULVOC, ELVOC, LVOC and SVOC denote ultra-low volatile organic compound, extremely low volatile organic compound, low volatile organic compound and semi-volatile organic compound, respectively.

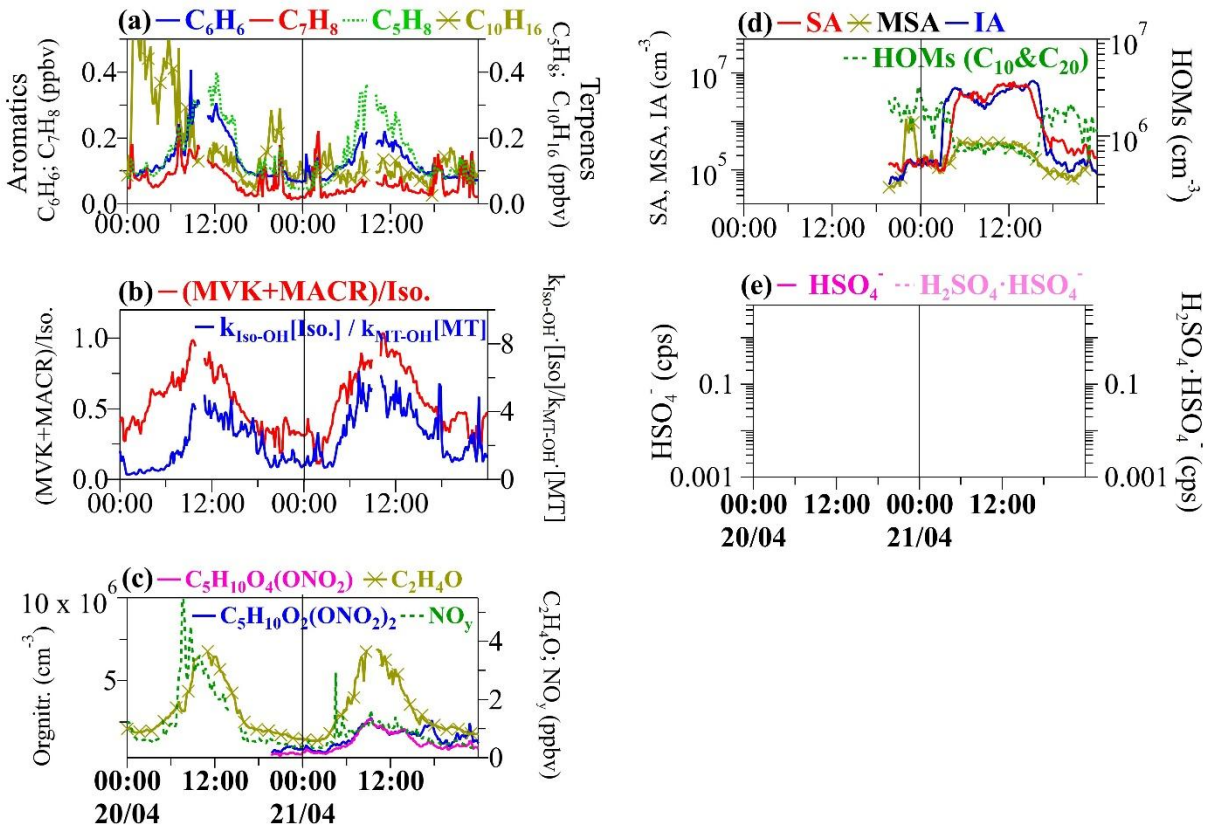

Figure S10. Same as Fig. S9, but for the consecutive NPF-NPS events observed during 20-21 April. MION-APi-TOF measurements are not available on 20-21 April.

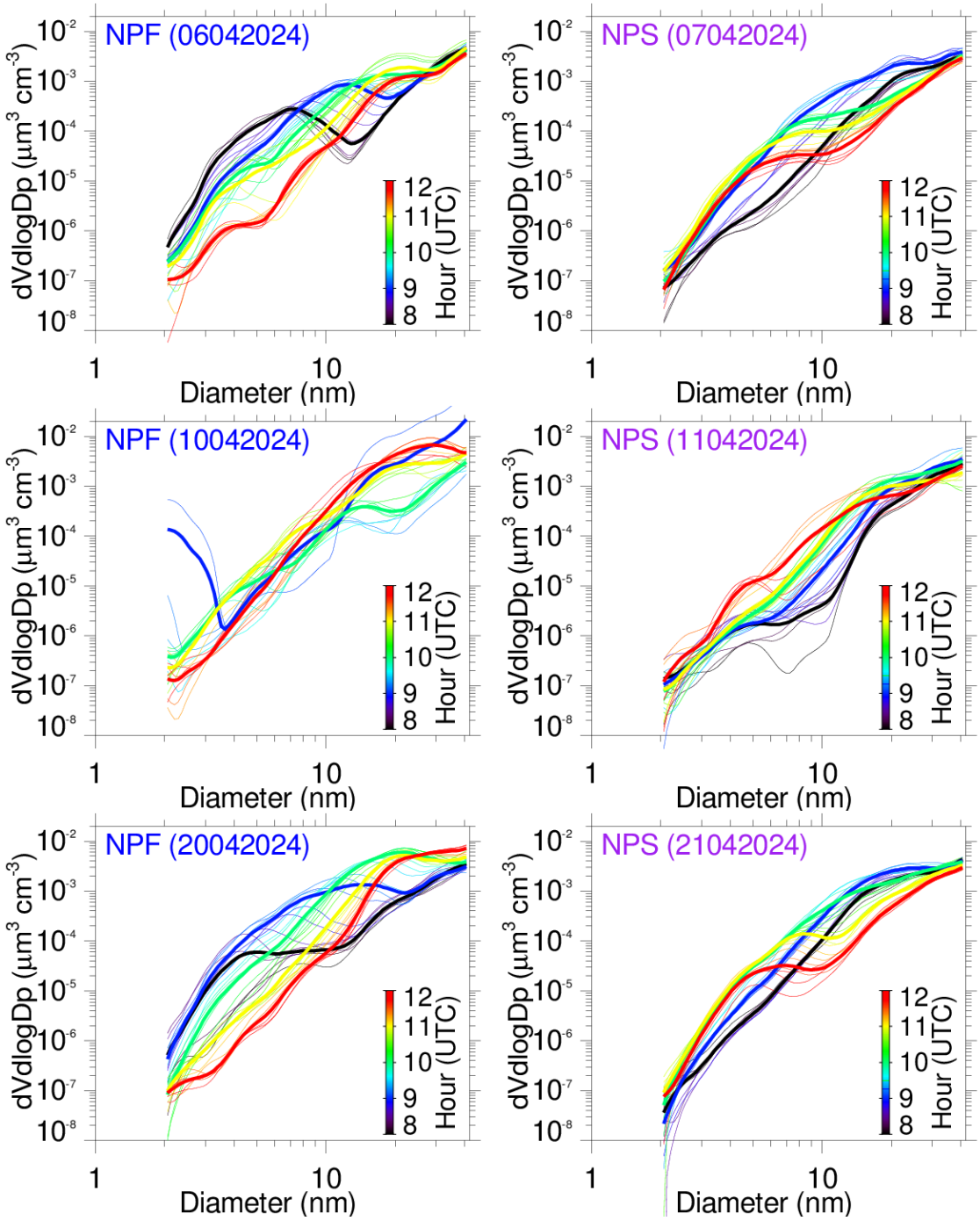

Figure S11. Ten-minute (thin lines) and hourly (thick lines) median particle volume size distribution (negative polarity) measured by the NAIS during the observed NPF (left column) and NPS (right column) events.

References

Hussein, T., Junninen, H., Tunved, P., Kristensson, A., Dal Maso, M., Riipinen, I., Aalto, P. P., Hansson, H. C., Swietlicki, E., and Kulmala, M.: Time span and spatial scale of regional new particle formation events over Finland and Southern Sweden, Atmos. Chem. Phys., 9, 4699-4716, 10.5194/acp-9-4699-2009, 2009.